https://doi.org/10.5194/gmd-2022-144
Preprint. Discussion started: 7 July 2022

Geoscientific Model Development Discussions

A new precipitation emulator (PREMU v1.0) for lower complexity models

Gang Liu[1], Shushi Peng[1*], Chris Huntingford[2], Yi Xi[1]

[1]Sino-French Institute for Earth System Science, College of Urban and Environmental Sciences, Peking University, Beijing, China
[2]UK Centre for Ecology and Hydrology, Wallingford, Oxfordshire OX10 8BB, United Kingdom

Correspondence to: Shushi Peng (speng@pku.edu.cn)

Abstract. Precipitation is a crucial component of the global water cycle. Rainfall features strongly affect societal activities and are closely associated with the functioning of terrestrial ecosystems. Hence predicting global and gridded precipitation under different emission scenarios is an essential output of climate change research, enabling a better understanding of future interactions between land biomes and climate change. Here, we provide a data-calibrated precipitation emulator (PREMU), offering a convenient and computationally effective way to better estimate and represent precipitation simulated by Earth system models (ESMs) under different user-prescribed emission scenarios. We construct the relationship between global/local precipitation and modes of global gridded temperature and find that the emulator shows a good performance in predicting historically observed precipitation from GSWP3. The ESM-specific emulator also estimates well the simulated precipitation of nine ESMs and under four dissimilar future scenarios of future atmospheric greenhouse gases (GHGs). Our ESM-specific emulator also reproduced well interannual fluctuations ($R = 0.82–0.93$, $p < 0.001$) of global land average precipitation (GLAP) simulated by the nine ESMs, as well as their trends and spatial patterns. The default configuration of our emulator only requires gridded temperature, also available from lower complexity models (LCMs) such as IMOGEN (Zelazowski et al., 2018) and MESMER (Beusch et al., 2022), which themselves are calibrated against ESMs. Therefore, our precipitation emulator can be directly coupled within other LCMs, for instance improving on the current simpler linear scaling of precipitation changes against global warming implicit in IMOGEN. The PREMU model has the opportunity to provide the driving conditions to model well the hydrological cycle, ecological processes, and their interactions with climate change. Critically the efficiency of LCMs allows them to make projections for many more potential future trajectories in atmospheric GHG concentrations than is possible with full ESMs, due to the high computational requirement of the latter. This flexibility makes LCMs an especially valuable tool for policymakers.

1 Introduction

Representing all the important Earth system processes, Earth system models (ESMs) are the primary tools to study the impact of greenhouse gas emissions on our climate (IPCC, 2013). However, there is a lack of sufficient computational power to run our most comprehensive, physically complete climate models for every application of interest (Nicholls et al.,2020), or for

https://doi.org/10.5194/gmd-2022-144
Preprint. Discussion started: 7 July 2022


Geoscientific Model Development Discussions

every potential future emissions scenario. Thus, more computationally efficient tools are needed for climate change research (Gasser et al., 2017).

Lower complexity models (LCMs) are common approaches to improve computational efficiency in climate change research (Gasser et al., 2017). By describing highly parameterized macro-properties of the climate system, LCMs are many orders of magnitude faster than full complexity Earth System Models (ESMs) (Nicholls et al., 2020). The simplest LCMs are Energy Balance Models (EBMs) that use multiple parameterized numerical models to estimate the changes in greenhouse gas concentrations, radiative forcing and then global land/ocean average temperature under different emission scenarios (Meinshausen et al., 2011; Nicholls et al., 2020). However, such global "box" models do not simulate the spatial pattern of temperature. Some more complex LCMs, such as IMOGEN and OSCAR, additionally emulate the spatial pattern of temperature through the pattern-scaling method. Pattern-scaling multiplies global temperature change by spatial patterns to give regional information (Zelazowski et al., 2018; Gasser et al., 2017; Huntingford et al., 2010). Recently, a spatially resolved emulator (MESMER) coupled with the emission-driven LCM (MAGICC) has been developed, which is found to reproduce the spatial pattern of temperature in ESMs better (Beusch et al., 2022). Other than temperature, however, it is still a challenge for LCMs to simulate well other climate variables such as precipitation under different emission scenarios (Gasser et al., 2017).

Projecting changes in precipitation is important. Precipitation is a crucial component of the water cycle (Eltahir and Bras, 1996; Trenberth et al., 2003; Sun et al., 2018), has key societal implications and is closely associated with the functioning of terrestrial ecosystems. Accurately emulating precipitation change is necessary to determine the climate response to different emission scenarios and to understand feedbacks to global warming via rainfall-dependent vegetation net primary productivity (Gasser et al., 2017). Until now, however, only two LCMs (IMOGEN and OSCAR) can emulate precipitation (Zelazowski et al., 2018; Gasser et al., 2017). IMOGEN emulates the gridded precipitation based on the regression relationship (by month and location) between gridded precipitation and global land average temperature (Zelazowski et al., 2018). OSCAR constructs the emulator by establishing the relationship between global average precipitation and global average temperature and radiative forcing, and then using the pattern-scaling method to deduce the gridded precipitation (Gasser et al., 2017). Nevertheless, the gridded precipitation estimated by the simple linear method is not reliable either in IMOGEN or in OSCAR; the gridded precipitation predicted by IMOGEN only explains less than 20% of variance of seasonal precipitation in most regions (Zelazowski et al., 2018) and OSCAR cannot capture the interannual variations of gridded precipitation across the globe at all (Gasser et al., 2017). This may be because 1) the global average temperature could not fully characterize local temperature and moisture recycling (Prein et al., 2017) and large-scale circulation (Shepherd, 2014; Fereday et al., 2018; Heinze-Deml et al., 2021); 2) there is at any given location a nonlinear relationship between local rainfall features and global warming (Allen and Ingram., 2002; Collins et al., 2013; Chadwick and Good, 2013). Hence models such as IMOGEN, that rely on linear pattern-scaling, by definition cannot fully capture expected future precipitation changes.

https://doi.org/10.5194/gmd-2022-144
Preprint. Discussion started: 7 July 2022


Geoscientific Model Development Discussions

To this end, we proposed a computationally efficient precipitation emulator (PREMU), which uses gridded temperature data as independent forcing variables to reconstruct the gridded precipitation. In Sect. 2 we described the datasets (both measurements and ESM-based) and the methods to construct the driving-data specific emulator for historical observation and each ESM in detail. We illustrated the emulator's ability to emulate the historical and future precipitation in Sect. 3. Finally, Sect. 4 discusses the strengths and caveats of our emulator.

2 Data and Methods

2.1 Observation datasets

To verify the ability to predict historical precipitation using the emulator proposed in this study, we first tested it against the precipitation dataset from Global Soil Wetness Project Phase 3 (GSWP3) (Kim, 2017a). The GSWP3 dataset is based on the 20th Century Reanalysis (20CR) version 2c (Compo et al., 2011), and has precipitation fields at a resolution of 2° × 2°. The GSWP3 data is dynamically downscaled using spectral nudging and bias-correction from the Global Precipitation Climatology Project and Climate Research Unit (Humphrey and Gudmundsson, 2019). This approach successfully keeps the low frequency signal of the two original reanalysis products, yet provides additional high frequency signals which are lacking in previous products (Kim, 2017a). GSWP3 also provides the other seven climate variables including air temperature (Tair), specific humidity, surface down welling long-wave radiation, surface down welling short-wave radiation, surface air pressure, and near-surface wind speed at a 0.5° × 0.5° spatial resolution from years 1901 to 2016. Here, with an emphasis on precipitation, we used Tair and precipitation from GSWP3 from period 1901 to 1950 to calibrate the emulator and from 1951 to 2016 to verify the emulator's performance in predicting historical precipitation.

2.2 Earth System Model data

To evaluate the emulator's performance in estimating future precipitation, we additionally used monthly precipitation and Tair for years 2015 to 2100 from nine ESMs operated under four Shared Socioeconomic Pathways (SSPs; SSP1-2.6, SSP2-4.5, SSP3-7.0, and SSP5-8.5; O'Neill et al., 2016). These ESMs are included in the 6th phase of the Coupled Model Intercomparison Project (CMIP6; Table 1). The SSP5-8.5 scenario represents the largest future change of GHG concentrations, compared to the other three SSPs (Hausfather and Peters, 2020), and so is associated with the largest variation in precipitation and Tair changes. Hence we used the precipitation and Tair from SSP5-8.5 to calibrate the emulator and the other three scenarios to verify the emulator's performance at reproducing ESMs. In addition, in view of the different responses of precipitation to the changes of Tair in different ESMs, we constructed the emulator for each ESM respectively. For comparison between different models, the precipitation and Tair from all nine ESMs are re-gridded to the resolution of 2.5° × 2.5° using the first-order conservative remapping technique (Jones, 1999).

https://doi.org/10.5194/gmd-2022-144
Preprint. Discussion started: 7 July 2022


Geoscientific Model Development Discussions

2.3 Methods

2.3.1 Calibration

Given the relatively poor linear relationship between global/gridded (i.e. local) precipitation and global land mean temperature (as noted in Zelazowski et al., 2018), we try to build a new emulator for precipitation. We still search for a relationship between precipitation change and some function of gridded Tair (Fig. 1), although more complex than simply linear in global temperature. Since precipitation is also not controlled by local temperature (Zhou et al., 2020), we seek links to features of Tair from all grid cells (10,368 at 2.5° × 2.5° resolution) across the globe to predict precipitation variation.

In this section, we set out underlying methods for our emulation of local precipitation by the principal component regression (PCR) approach, based on relating it to the dominant modes of variability of temperature. PCR is a type of regression analysis, which considers the orthogonal principal components as independent variables. As a method that can be used to overcome the problem of multilinearity on predictor variables, PCR is widely used in forecasting seasonal precipitation (Kim et al.,2017b) and reconstructing the climatic modes of variability (Jones et al., 2009; Michel et al., 2020) and performed remarkably well. As might be expected, therefore, our starting point is deriving the principal components of global gridded temperature. We followed the standard procedure of Principal Component Analysis (PCA), as used in climate research, consisting of a set of time-invariant spatial patterns multiplied by timeseries. PCA notation can vary between users, but for simplicity, we will simply refer to these as PCA "spatial patterns" (each of which has the dimensions of the spatial grid, or alternatively an array of one dimension with 10,368 points), and PCA "timeseries", which multiply the patterns. These timeseries, derived for each month, contain values applicable for each year, and so for instance, fitting to years 1901-1950 imply they will have 50 numbers. As precipitation may be influenced by the temperature of the previous months, we used the average Tair of three months (month of interest plus the previous two months) to apply PCA. In addition, considering that ESM may under-represent the effects of topography and aerosols on the precipitation from observations, we calibrated the emulator for the historical period and future respectively. For the future, we used precipitation and Tair from SSP5-8.5 to calibrate the ESM-specific emulator due to its largest changes in Tair covering the range of other SSPs. The detailed reasons for using precipitation and Tair from SSP5-8.5 rather than other lower emission scenarios or historical period are discussed in the Sect. **4**.

We set out in the Table 2 below our notation for indices and variable quantities.

Our use of the standard definition of PCAs (sum of patterns × timeseries) implies that the estimate of the principal components is given by the spatial pattern of principal component coefficients $U_{e,m}^{Spatial}(k,i)$ multiplied by the timeseries of three months average gridded temperature. However, unlike many limited-area applications that derive a single timeseries (to multiply each PCA), we instead determined a timeseries for each location, and hence why $T_{e,m}^{Timeseries}(k,y)$ has a k dependency. We then summed over all locations k, and this gives a global annual timeseries (for each month m, and PCA i) of:

$$T_{e,m}^{PCA}(y,i) = \sum_{k=1}^{N_{grid}} U_{e,m}^{Spatial}(k,i) * T_{e,m}^{Timeseries}(k,y) \quad (1)$$

https://doi.org/10.5194/gmd-2022-144
Preprint. Discussion started: 7 July 2022


Geoscientific Model Development Discussions

Using Tair for years 1901-1950 from the GSWP3 gridded dataset, and for period 2016-2100 from the nine ESMs forced under the SSP5-8.5 scenario, we determined the principal component coefficient matrix $U_{e,m}^{Spatial}$ for each month m, and ESM e (or GWSP3) independently. We employed Equation (1), and the top 10 principal components (i = 1,…,10) were used in this study, which described more than 70% of gridded temperature information (i.e. variation) across the globe (Fig. 2 and Figs. S1-S3).

Having established the temperature principal components, via the form presented in Eq (1), we then mapped these onto precipitation both globally and locally. Our mapping is via a standard regression based on 50 datapoints (i.e. year 1901-1950; or 86 datapoints in ESMs for year 2015-2100). The regression has 10 degrees-of-freedom, due to our selection of 10 PCAs, and this relationship links the timeseries of global monthly GLAP from the GSWP3 dataset (or the nine ESMs) and the 10 principal components of gridded temperature for each month of the 12 months of the year (January to December). This regression is constructed as:

$$P_{e,m}^{global}(y) = \sum_{i=1}^{N_{PCA}} \alpha_{e,m}(i) * T_{e,m}^{PCA}(y,i) + \alpha_{e,m}^{intercept}(i) \quad (2)$$

where $P_{e,m}^{global}$ is the monthly GLAP. $\alpha_{e,m}$ represents the regression coefficient of each principal component and $\alpha_{e,m}^{intercept}$ is the intercept term, which are derived from linear regressions by least squares fitting. To provide the spatial pattern of monthly precipitation, we also constructed the local (i.e. spatial) regression relationship between gridded precipitation and the 10 individual principal components as:

$$P_{e,m}^{grid}(k,y) = \sum_{i=1}^{N_{PCA}} \beta_{e,m}(k,i) * T_{e,m}^{PCA}(y,i) + \beta_{e,m}^{intercept}(k,i) \quad (3)$$

and where $P_{e,m}^{grid}(k,y)$ is the precipitation at a specific cell, k. Variable $\beta_{e,m}$ represents the regression coefficient of each principal component and $\beta_{e,m}^{intercept}$ is the intercept term, which are derived from linear regressions by least squares method using the calibration time series.

2.3.2 Validation

For validation, we set out in the table below the variables that we estimate with our methodology. The "overhat" notation represents an estimated quantity.

Variable Symbol	Variable	Notes
$\widehat{T_{e,m}^{PCA}(y,i)}$	Principal components estimated by the Tair from validation datasets	Based on the assumption of constant spatial part of PCAs, $U_{e,m}^{Spatial}(k,i)$.
$\widehat{P_{e,m}^{global}(y)}$	Estimation of monthly global precipitation, GLAP	
$\widehat{P_{e,m}^{grid}(k,y)}$	Estimation of monthly gridded (i.e. spatial) precipitation	

https://doi.org/10.5194/gmd-2022-144
Preprint. Discussion started: 7 July 2022

Geoscientific Model Development Discussions

We first recalled that we fitted our PCA-based framework to historical temperature and precipitation data for period 1901-1950, and to ESMs for the SSP5-8.5 future atmospheric GHG concentration scenario. Based on the principal component coefficients extracted using these calibration datasets, we then estimated the $\widehat{T_{e,m}^{PCA}(y,\iota)}$ for 1951-2016 using Tair from GSWP3 and for 2015-2100 using Tair from each ESM independently under the other three SSPs:

$$\widehat{T_{e,m}^{PCA}(y,\iota)} = \sum_{k=1}^{N_{grid}} U_{e,m}^{Spatial}(k,i) * T_{e,m}^{Timseries,val}(k,y), \quad (4)$$

Then we estimated the $\widehat{P_{e,m}^{global}(y)}$ and $\widehat{P_{e,m}^{grid}(s,y)}$ by the $\widehat{T_{e,m}^{PCA}(y,\iota)}$ and our fitted regression coefficients in Eq. 2 and Eq. 3:

$$\widehat{P_{e,m}^{global}(y)} = \sum_{i=1}^{N_{PCA}} \alpha_{e,m}(i) * \widehat{T_{e,m}^{PCA}(y,\iota)} + \alpha_{e,m}^{intercept}(i), \quad (5)$$

$$\widehat{P_{e,m}^{grid}(k,y)} = \sum_{i=1}^{N_{PCA}} \beta_{e,m}(k,i) * \widehat{T_{e,m}^{PCA}(y,\iota)} + \beta_{e,m}^{intercept}(k,i), \quad (6)$$

where the $T_{e,m}^{Timseries,val}$ is the gridded Tair from validation datasets, and as before is the average of the previous three months. We found a slight difference in GLAP between $\widehat{P_{e,m}^{global}}$ and the spatial average of $\widehat{P_{e,m}^{grid}}$, but $\widehat{P_{e,m}^{global}}$ had a slightly better correlation with GSWP3. Thus, in a final component to our calculations, we scale $\widehat{P_{e,m}^{grid}}$ by the ratio of $\widehat{P_{e,m}^{global}}$ and the monthly GLAP from area-weighted averaged $\widehat{P_{e,m}^{grid}}$, i.e. with equation:

$$\widehat{P_{e,m}^{grid,Adj}}(k,y) = \widehat{P_{e,m}^{grid}}(k,y) * \frac{\widehat{P_{e,m}^{global}}}{Mean\left(\widehat{P_{e,m}^{grid}}\right)}, \quad (7)$$

where $\widehat{P_{e,m}^{grid,Adj}}$ is the adjusted estimation of monthly gridded precipitation and $Mean\left(\widehat{P_{e,m}^{grid}}\right)$ represents the area-weighted averaged $\widehat{P_{e,m}^{grid}}$.

3 Results

3.1 Performance of precipitation emulator on historical precipitation

As outlined above, to evaluate the ability of our PREMU to emulate historical precipitation, we first used the precipitation and Tair data from GSWP3, for the period 1901-1951, to calibrate its parameters. We then tested its predictive capability at estimating precipitation data from the period 1951-2016. For the calibration period (1901-1950), our emulator shows a consistent areally-averaged global annual precipitation value (1002 mm year^{-1} and 1002 mm year^{-1} for PREMU and GSWP3, respectively) and trend (0.48 mm year^{-2} and 0.54 mm year^{-2} for PREMU and GSWP3). Furthermore, the interannual variations of GLAP derived from PREMU are found to be significantly correlated with that from GSWP3 ($R = 0.81$, $p < 0.001$). For the validation period (1951-2016), PREMU also captured the observed trend (0.22 mm year^{-2} for both PREMU and GSWP3) and interannual variations ($R = 0.67$, $p < 0.001$) of GLAP from GSWP3 (Fig.3a). By contrast, if we simply used a prediction that

https://doi.org/10.5194/gmd-2022-144
Preprint. Discussion started: 7 July 2022


Geoscientific Model Development Discussions

linearly relates rainfall changes to global temperature changes and variability, which has similarities to the IMOGEN-based method, we found a much smaller (-0.25 mm year^{-2}, -45%) and larger (+0.47 mm year^{-2}, +213%) trend in GLAP than GSWP3 for the calibration and validation periods, respectively. In addition, the interannual variations of GLAP as estimated by a simple linear regression against global temperature, shows a weaker correlation with GSWP3 in these two periods ($R = 0.27$, $p = 0.06$ for the calibration period; $R = 0.15$, $p = 0.21$ for validation period; Fig. 3a).

Spatially, PREMU and a simple linear-based method (similar to the algorithms in IMOGEN) can both emulate similarly the spatial pattern of mean annual precipitation (MAP) during the last three decades in the validation period (1987–2016), as observed in the GSWP3 data (Fig. 4a, c, e). Compared to the simple linear approach, there are fewer grid cells showing more than 25% error of MAP from GSWP3 in our emulation (17%) against a simple linear fit (27%; Fig. 3b,c). The overestimation of MAP with our PREMU method is mainly found in the Tibetan Plateau and central Africa (~20%), and the underestimation of MAP mainly in northern Siberia, Greenland Island and northern Australia (-15% – -30%); Fig. 3c). To verify the emulator's ability to predict changes in gridded observation precipitation, we calculated the change of MAP in the first and last three decades of the validation period (1951-1980 and 1987-2016; Fig. 4b, d, f). For the differences between these two time periods, both PREMU and GSWP3 consistently show an increase of annual precipitation in the northern Eurasia, North America and the southern South America and a decrease in central South America. However, in some regions of East Asia, Europe, Australia and South America, PREMU underestimates / overestimates the changes in annual precipitation (50–200 mm year^{-1}; Fig. 4).

3.2 Performance of precipitation emulator on future precipitation from CMIP6 ESMs

A key requirement of our PREMU emulator is that it can make projections of precipitation change for different future scenarios of atmospheric GHG concentrations, and potentially for novel trajectories of such gases for which ESMs have not made calculations. To test for this capability, we analysed its performance at predicting changes under the SSP1-2.6, SSP2-4.5 and SSP3-7.0 scenarios, and for which ESM-based simulations that are available. Recall that our PREMU calibration was against ESMs operated for the SSP5-8.5 scenario, capturing inter-ESM differences in projections of Tair, and critically, precipitation. Similar to the emulation for the historical period, PREMU shows a good performance in emulating future precipitation (Fig. 5). For the calibration scenario, the multi-model mean GLAP from PREMU shows consistent trend (0.96 mm year^{-2} and 0.96 mm year^{-2} for our emulator and ESMs) and interannual variation ($R = 0.98$, $p<0.001$) with that from ESMs (Fig. 5a). For the three validation scenarios of the different SSPs, PREMU shows a better correlation in interannual variations of GLAP with ESMs than the historical period ($R = 0.86$, $p<0.001$ for SSP1-2.6; $R = 0.95$, $p<0.001$ for SSP2-4.5; $R = 0.95$, $p<0.001$ for SSP3-7.0; Fig. 5c,e,g). Although the trends of global precipitation in our emulation are close to that of ESMs across the three scenarios (Table 3), the error of trends by the PREMU increases from high to low emission scenarios. Hence, we found larger errors when interpolating to colder climates using the emulator constructed under a high emissions scenario (SSP5-8.5). At the individual ESM level, PREMU can capture well both trends and interannual fluctuations of GLAP well under all scenarios for MPI-ESM1-2-LR, MIROC6, EC-Earth3 and CanESM5. For the other five models, there are biases of trends (Table 3)

https://doi.org/10.5194/gmd-2022-144
Preprint. Discussion started: 7 July 2022


Geoscientific Model Development Discussions

and/or interannual variations of GLAP (Fig. 6 and Figs. S4-S6) between our emulation and ESMs. These differences could be partly related to the substantial uncertainties in future precipitation projection in ESMs.

For the spatial pattern (Fig. 5b,d,f,h), PREMU can reproduce the projected pattern of MAP from the multi-model mean of ESMs under the calibration scenario and the three validation scenarios (Fig. 7). Compared to the historical period, the error of multi-model MAP between our emulation and ESMs is relatively smaller (~10%; Fig. 7). During the prediction period, defined here as years 2015-2100, PREMU predicts a 50-200 mm year^{-1} increase of annual precipitation in Eurasia, North America and northeastern of Africa, but a 50-200 mm years^{-1} decrease in Amazon rainforest from the low to high emission scenarios, which is consistent with the canonical pattern from the multi-model mean of ESMs (Fig. 8). Similar to the simulation for GLAP, the error in spatial pattern of MAP and changes in MAP between our emulation and ESMs increases from high to low emission scenarios (Fig. 5 and Fig. 8). Under the SSP3-7.0 scenario, PREMU shows a less than 100 mm year^{-1} error of change in MAP in 64% of grid cells. While under the lowest emission scenario (SSP1-2.6), PREMU underestimates the increase of MAP in eastern China (100-200 mm year^{-1}) and overestimates the decrease in southern Europe (50-100 mm year^{-1}). When considering performance at the individual ESM level, PREMU can reproduce the spatial pattern of MAP well. In general, the proportions of grid cells with an error more than 10% is small (8% [6%-14%] for SSP1-2.6; 5% [3%-8%] for SSP2-4.5; 5% [3%- 9%] for SSP3-7.0; 0% [0%- 0 %] for SSP5-8.5; mean [min-max]; Fig. 9 and Figs. S7-S9). However, as for the changes in MAP, we found a relative poor performance in emulating the changes in some ESMs especially in SSP1-2.6 (Fig. 10 and Figs. S10-S12). While the spatial pattern of changes in MAP is quite different across ESMs even under the same SSP, the errors by PREMU are much smaller than the inter-ESM differences (Fig. 10 and Figs. S10-S12).

4 Discussion

To our knowledge, this study provides a novel approach to linking local precipitation changes to geographical features (i.e. spatial modes) of gridded temperature in a single emulator chain, which can be further incorporated into existing LCMs. Despite relying on a series of simple assumptions, PREMU can successfully capture the simulated changes in precipitation by ESMs and under a broad range of different emission scenarios. Comparing with the precipitation predicted by a simple linear regression between local rainfall alteration and level of global warming (e.g. as used in other LCMs such as IMOGEN), the rainfall in PREMU shows more consistent trends and interannual variations of GLAP and in the spatial pattern of MAP. These improvements are noted in the comparison against the historical precipitation recorded in the GSWP3 dataset, as well as when emulating the predicted future precipitation by ESMs (Figs. 3-6). For a user-prescribed emission scenario, or for a time-evolving global temperature trajectory designed to constrain warming to a level such as two degrees (Huntingford et al., 2017), PREMU can accurately and quickly emulate the related gridded precipitation changes. Our method can utilize the existing spatial features of gridded temperature from either ESMs or LCMs, to support studies related to future changes in precipitation. In particular, coupling our precipitation emulator with other LCMs provides the input climate forcing for land surface models

https://doi.org/10.5194/gmd-2022-144
Preprint. Discussion started: 7 July 2022

to help disentangle hydrological and ecological responses globally to future climate change (Zelazowski et al., 2018; Li et al., 2022; Korell et al., 2021).

We note that the performance of PREMU at predicting future precipitation from ESMs is much better than that when emulating historical GSWP3 precipitation. This is because PREMU is only based on the ten modes of global gridded temperature, and the effects of aerosols and topography on precipitation are not well represented in our emulator (Austin and Dirks., 2005; Medvigy et al., 2012). For instance, Fig. 3 shows emulated precipitation has large errors in mountainous regions, where orographic precipitation could be dominant. The effect of raised aerosols in the 20th century have been shown as having a role almost as large as greenhouse gases warming effects on features of regional precipitation (e.g. in India; Bollasina et al., 2011). Thus, adding the effects of topography and aerosols on precipitation in to the PREMU could further improve the ability of predicting precipitation. An alternative argument is that the good performance on predicting precipitation from ESMs by PREMU may suggest that climate models under-represent the effects of topography and aerosols (Samset et al., 2016; Yang et al., 2021).

Overall, the performance of predicting precipitation from ESMs by our emulator is good, although not for all models and under all scenarios. Both trends and interannual variability of GLAP are well captured under all scenarios for MPI-ESM1-2-LR, MIROC6, EC-Earth3 and CanESM5, but PREMU performs less well at predicting GLAP in the other five ESMs (Fig. 6 and Figs. S4-S6). This may be because different ESMs use alternative atmospheric circulation model and precipitation schemes (e.g., CAM6.3 in CESM2 and AM4 in GFDL-ESM4), which contain different physical processes or parameterizations in their simulation of precipitation (Danabasoglu et al., 2020; Horowitz et al., 2020; Hourdin et al., 2020). Notable is that, PREMU underestimates 30% (6%–60%) of interannual variations of precipitation in all ESMs and when considering across all four GHG concentration scenarios. This is a common “feature” of linear regression models, as they favor bias reduction over variance under the bias-variance trade-off (Geman et al.,1992). In addition, we also suggest this may be because of missing some modes (out of the 10 modes we used) for interannual variations, or an under-representation of the effect of key climate modes such as ENSO in our emulator, or a non-linear response of precipitation to climate modes. It is also worth noting that the trend of GLAP in CESM2 and GFDL-ESM4 under SSP3-7.0 are lower than that under SSP2-4.5. We speculate that this may be caused by the most drastic land use changes of that former SSP, and that are account for in ESM simulations, resulting in a slower increase in precipitation under SSP3-7.0 (Riahi et al., 2017). Our emulator predicts precipitation through the temperature gradients and so cannot capture the impact of land-use changes on precipitation via altered land-atmospheric feedbacks impacts the hydrological cycle (Table 3).

Our emulator is based on the assumption that spatial temperature modes can describe well precipitation. Hence, we assumed implicitly that the coefficient matrix in PCA for global gridded temperature (i.e., the weights of each grid cell for each principal component) are stable, i.e. invariant, with climate change. To test this assumption, we compared the coefficient matrixes of

https://doi.org/10.5194/gmd-2022-144
Preprint. Discussion started: 7 July 2022

temperature derived for the SSP5-8.5 scenario with those from the SSP1-2.6 scenario, for modelled period 2015-2100 (Figs. S13 and S14). For the future scenarios, we found that most coefficients of PCA, in both January and July, are similar between the SSP5-8.5 scenario and SSP1-2.6 scenario, explaining >95% variations in global temperature. This is, though, with a different order of PCA coefficients (for example, the third PCA of SSP5-8.5 in Fig. S3d corresponds to the second PCA of SSP1-2.6 in Fig. S14c; Figs. S2-S3, S13-S14). This finding suggests that the main features of global temperature are constant across different scenarios. We note in some instances, the signs of coefficients are opposite for some principal components between different scenarios, but this corresponds to regression coefficients also with opposite signs, which combined give the same predictions.

We have confirmed that our ability to reproduce the historical and future trends as well as interannual variabilities in precipitation, is better than with other methods that more simply regression local changes against global temperature variation (e.g. IMOGEN and OSCAR; Zelazowski et al., 2018; Gasser et al., 2017). However, the remaining biases in emulating the other three SSPs with the emulator constructed (i.e. fitted) under SSP5-8.5 imply that the sensitivity of gridded precipitation to temperature modes may have a slight dependence on SSP. There are some studies predict that the variability of precipitation will increase in a warmer world (Zhang et al., 2021; Song et al., 2018), but where such additional variability is not present in the spatial temperature modes of variations. Therefore, it could be unwise to use the emulator constructed using the temperature and precipitation during the historical period or under the low emission scenarios to project future precipitation change under a high emission scenario. Constructing the emulator separately for low or high emission scenarios could help reduce uncertainties in emulating future precipitation.

We tested the effect of different lags of gridded temperature on changes in precipitation. Previous studies noted that "memory effects" may cause precipitation to be affected more by the climate modes in the previous months (An et al., 2020). Here, we used throughout the three-month average temperature (month of interest plus the previous two months) to capture potential lagging effects. However, to quantify the uncertainty based on duration of the lag effect, we also tested one-month temperature and six-month average temperature to construct the emulator respectively ("emulator-1mon" and "emulator-6mon"). For the historical period, we found that the emulator-1mon was unable to capture the increase of GLAP after 1950. Predicting the GLAP from emulator-6mon shows a good fitting of the trends and interannual variations of GLAP in GSWP3 similar to that from emulator based on three-month average temperature, but with a lower correlation coefficient ($R=0.77$, $p<0.001$ for three-month; $R=0.73$, $p<0.001$ for six-month; Fig. S15). While for future precipitation from ESMs, all three emulators with different temperature lag periods (one-month, three-month, six-month) can capture well the changes in GLAP and gridded precipitation under different scenarios in the future (Fig. S16, S17). Hence, we deduce that the method is highly robust (i.e. invariant) to lag-length when emulating the future precipitation (Fig. 5 and Fig. S16-17).

https://doi.org/10.5194/gmd-2022-144
Preprint. Discussion started: 7 July 2022


Geoscientific Model Development Discussions

We constructed our emulator using thermal modes of variation based on the temperature from over both land and ocean grid cells. As a sensitivity study, we also evaluated the performance of the emulator constructed only using Tair over land ("emulator-land") to test its capability at predicting future precipitation. We found that the emulator-land can also reproduce consistent trends and interannual variations of GLAP and changes in gridded precipitation with ESMs (Fig. S18 and S19). However, considering that the change of air temperature over ocean could contain additional information that relates to local climate variability (Trenberth and Shea, 2005), we suggest retaining our inclusion of all land and ocean grid cells in PREMU calibration.

Our emulator has focused on total precipitation at each location. Future analyses could include testing its performance for individual features or subsets of precipitation patterns, such as convective precipitation, large-scale precipitation and topographic precipitation. We also suggest possibly extending our emulator drivers beyond the modes of variability of air temperature only. For example, considering that the interannual variations of precipitation are mainly caused by large-scale precipitation dominated by ESNO (Cai et al., 2001; Oldenborgh and Burgers, 2005; Gupta and Jain., 2021; Zhou et al., 2020), we could consider additionally entraining sea surface temperature as a forcing variable. Similarly, for convective precipitation, local temperature and energy for uplift could be used for prediction (Berg et al., 2013).

5 Conclusions

In this study, we proposed an algorithm to construct a precipitation emulator, which could estimate gridded precipitation and its changes in a convenient and computationally effective way. We exploit strong discovered linkages between rainfall patterns and natural spatial modes of variability in near-surface temperature. To the best of our knowledge, this is a pioneer emulator that can be directly coupled within existing LCMs, and especially noting that LCMs may perform well for other variables but are currently weaker at estimating features of rainfall. This new combination will better predict global and gridded precipitation under different emission scenarios. With illustrative examples, we demonstrated the good performance of our emulator in predicting the absolute value and interannual variations in historical precipitation from GSWP3 as well as predicted future precipitation under four scenarios from ESMs. In addition, we also verified the reliability of our results despite the potential uncertainties in the method (e.g., the assumptions of the stability in coefficient matrix in PCA and sensitivity of gridded precipitation to temperature modes). The accurate projection of future precipitation can help analyze not only expected direct climate change under different emission scenarios but also the responses of the hydrological cycle and ecological processes to such future changes. ESMs remain hugely computationally demanding and can be only operated for a limited number of century-timescale projections. Hence robust emulators of full-complexity Earth system models remain an important tool, extrapolating ESM projections to alternative future emissions or GHG concentration scenarios that require investigation and understanding.

https://doi.org/10.5194/gmd-2022-144
Preprint. Discussion started: 7 July 2022


Geoscientific Model Development Discussions

Code availability

The MATLAB code used to emulate the precipitation by PREMU is publicly available on GitHub (https://github.com/GangLiulg/PreMU), and the code used here is achieved and available on Zenodo repository (https://doi.org/10.5281/zenodo.6668938).

Data availability

The GSWP3 data were available at http://search.diasjp.net/en/dataset/GSWP3_EXP1_Forcing. All CMIP6 data can be accessed from the CMIP6 archive (https://esgf-node.llnl.gov/search/cmip6/).

Author contributions

SP conceived this study. The PREMU model was coded and developed mainly by GL. GL, SP and YX prepared the paper with contributions from CH.

Competing interests

The contact author has declared that neither they nor their co-authors have any competing interests.

Acknowledgements

The authors would like to thank Data Integration and Analysis System (DIAS), Japan manage publicly availability of GSWP3, and CMIP6 data producers and providers.

Financial support

This development has been supported by the National Natural Science Foundation of China (grant numbers 41722101 and 41830643).

References

Allen, M. R. and Ingram, W. J.: Constraints on future changes in climate and the hydrologic cycle, Nature, 419, 228-232, 10.1038/nature01092, 2002.

https://doi.org/10.5194/gmd-2022-144
Preprint. Discussion started: 7 July 2022

An, L., Hao, Y., Yeh, T.-C. J., and Zhang, B.: Annual to multidecadal climate modes linking precipitation of the northern and southern slopes of the Tianshan Mts, Theor. Appl. Climatol., 140, 453-465, 10.1007/s00704-020-03100-y, 2020.

Austin, G. L. and Dirks, K. N.: Topographic Effects on Precipitation, in: Encyclopedia of Hydrological Sciences, https://doi.org/10.1002/0470848944.hsa033, 2005.

Berg, P., Moseley, C., and Haerter, J. O.: Strong increase in convective precipitation in response to higher temperatures, Nat. Geosci., 6, 181-185, 10.1038/ngeo1731, 2013.

Beusch, L., Nicholls, Z., Gudmundsson, L., Hauser, M., Meinshausen, M., and Seneviratne, S. I.: From emission scenarios to spatially resolved projections with a chain of computationally efficient emulators: coupling of MAGICC (v7.5.1) and MESMER (v0.8.3), Geosci. Model Dev., 15, 2085-2103, 10.5194/gmd-15-2085-2022, 2022.

Bollasina, M. A., Ming, Y., and Ramaswamy, V.: Anthropogenic Aerosols and the Weakening of the South Asian Summer Monsoon, Science, 334, 502-505, doi:10.1126/science.1204994, 2011.

Cai, W., Whetton, P. H., and Pittock, A. B.: Fluctuations of the relationship between ENSO and northeast Australian rainfall, Clim. Dynam., 17, 421-432, 10.1007/PL00013738, 2001.

Chadwick, R. and Good, P.: Understanding nonlinear tropical precipitation responses to CO2 forcing, Geophys. Res. Lett., 40, 4911-4915, https://doi.org/10.1002/grl.50932, 2013.

Collins, M., Knutti, R., Arblaster, J., Dufresne, J. L., Fichefet, T., Friedlingstein, P., Gao, X., Gutowski, W. J., Johns, T., Krinner, G., Shongwe, M., Tebaldi, C., Weaver, A. J., and Wehner, M.: Long-term Climate Change: Projections, Commitments and Irreversibility, in: Climate Change 2013: The Physical Science Basis, Contribution of Working Group I to the Fifth Assessment Report of the Intergovernmental Panel on Climate Change, edited by: Stocker, T. F., Qin, D., Plattner, G. K., Tignor, M., Allen, S. K., Boschung, J., Nauels, A., Xia, Y., Bex, V., Midgley, P. M., Cambridge University Press, Cambridge, UK, New York, NY, USA, 2013.

Compo, G. P., Whitaker, J. S., Sardeshmukh, P. D., Matsui, N., Allan, R. J., Yin, X., Gleason, B. E., Vose, R. S., Rutledge, G., Bessemoulin, P., Brönnimann, S., Brunet, M., Crouthamel, R. I., Grant, A. N., Groisman, P. Y., Jones, P. D., Kruk, M. C., Kruger, A. C., Marshall, G. J., Maugeri, M., Mok, H. Y., Nordli, Ø., Ross, T. F., Trigo, R. M., Wang, X. L., Woodruff, S. D., and Worley, S. J.: The Twentieth Century Reanalysis Project, Q. J. R. Meteorol. Soc., 137, 1-28, https://doi.org/10.1002/qj.776, 2011.

Danabasoglu, G., Lamarque, J.-F., Bacmeister, J., Bailey, D. A., DuVivier, A. K., Edwards, J., Emmons, L. K., Fasullo, J., Garcia, R., Gettelman, A., Hannay, C., Holland, M. M., Large, W. G., Lauritzen, P. H., Lawrence, D. M., Lenaerts, J. T. M., Lindsay, K., Lipscomb, W. H., Mills, M. J., Neale, R., Oleson, K. W., Otto-Bliesner, B., Phillips, A. S., Sacks, W., Tilmes, S., van Kampenhout, L., Vertenstein, M., Bertini, A., Dennis, J., Deser, C., Fischer, C., Fox-Kemper, B., Kay, J. E., Kinnison, D., Kushner, P. J., Larson, V. E., Long, M. C., Mickelson, S., Moore, J. K., Nienhouse, E., Polvani, L., Rasch, P. J., and Strand, W. G.: The Community Earth System Model Version 2 (CESM2), J. Adv. Model. Earth Syst., 12, e2019MS001916, https://doi.org/10.1029/2019MS001916, 2020.

https://doi.org/10.5194/gmd-2022-144
Preprint. Discussion started: 7 July 2022

395 Eltahir, E. A. B. and Bras, R. L.: Precipitation recycling, Rev. Geophys, 34, 367-378, https://doi.org/10.1029/96RG01927, 1996.

Fereday, D., Chadwick, R., Knight, J., and Scaife, A. A.: Atmospheric Dynamics is the Largest Source of Uncertainty in Future Winter European Rainfall, J. Climate, 31, 963-977, 10.1175/jcli-d-17-0048.1, 2018.

Gasser, T., Ciais, P., Boucher, O., Quilcaille, Y., Tortora, M., Bopp, L., and Hauglustaine, D.: The compact Earth system
400 model OSCAR v2.2: description and first results, Geosci. Model Dev., 10, 271-319, 10.5194/gmd-10-271-2017, 2017.

Geman, S., Bienenstock, E., and Doursat, R.: Neural Networks and the Bias/Variance Dilemma, Neural Comput., 4, 1-58, 10.1162/neco.1992.4.1.1, 1992.

Gupta, V. and Jain, M. K.: Unravelling the teleconnections between ENSO and dry/wet conditions over India using nonlinear Granger causality, Atmos. Res., 247, 105168, https://doi.org/10.1016/j.atmosres.2020.105168, 2021.

405 Heinze-Deml, C., Sippel, S., Pendergrass, A. G., Lehner, F., and Meinshausen, N.: Latent Linear Adjustment Autoencoder v1.0: a novel method for estimating and emulating dynamic precipitation at high resolution, Geosci. Model Dev., 14, 4977-4999, 10.5194/gmd-14-4977-2021, 2021.

Horowitz, L. W., Naik, V., Paulot, F., Ginoux, P. A., Dunne, J. P., Mao, J., Schnell, J., Chen, X., He, J., John, J. G., Lin, M., Lin, P., Malyshev, S., Paynter, D., Shevliakova, E., and Zhao, M.: The GFDL Global Atmospheric Chemistry-Climate
410 Model AM4.1: Model Description and Simulation Characteristics, J. Adv. Model. Earth Syst., 12, e2019MS002032, https://doi.org/10.1029/2019MS002032, 2020.

Hourdin, F., Rio, C., Grandpeix, J.-Y., Madeleine, J.-B., Cheruy, F., Rochetin, N., Jam, A., Musat, I., Idelkadi, A., Fairhead, L., Foujols, M.-A., Mellul, L., Traore, A.-K., Dufresne, J.-L., Boucher, O., Lefebvre, M.-P., Millour, E., Vignon, E., Jouhaud, J., Diallo, F. B., Lott, F., Gastineau, G., Caubel, A., Meurdesoif, Y., and Ghattas, J.: LMDZ6A: The Atmospheric
415 Component of the IPSL Climate Model With Improved and Better Tuned Physics, J. Adv. Model. Earth Syst., 12, e2019MS001892, https://doi.org/10.1029/2019MS001892, 2020.

Humphrey, V. and Gudmundsson, L.: GRACE-REC: a reconstruction of climate-driven water storage changes over the last century, Earth Syst. Sci. Data, 11, 1153-1170, 10.5194/essd-11-1153-2019, 2019.

Huntingford, C., Yang, H., Harper, A., Cox, P. M., Gedney, N., Burke, E. J., Lowe, J. A., Hayman, G., Collins, W. J., Smith,
420 S. M., and Comyn-Platt, E.: Flexible parameter-sparse global temperature time profiles that stabilise at 1.5 and 2.0 °C, Earth Syst. Dynam., 8, 617-626, 10.5194/esd-8-617-2017, 2017.

Huntingford, C., Booth, B. B. B., Sitch, S., Gedney, N., Lowe, J. A., Liddicoat, S. K., Mercado, L. M., Best, M. J., Weedon, G. P., Fisher, R. A., Lomas, M. R., Good, P., Zelazowski, P., Everitt, A. C., Spessa, A. C., and Jones, C. D.: IMOGEN: an intermediate complexity model to evaluate terrestrial impacts of a changing climate, Geosci. Model Dev., 3, 679-687,
425 10.5194/gmd-3-679-2010, 2010.

IPCC: Climate Change 2013: The Physical Science Basis, Contribution of Working Group I to the Fifth Assessment Report of the Intergovernmental Panel on Climate Change, edited by: Stocker, T. F., Qin, D., Plattner, G.-K., Tignor, M., Allen, S.

K., Boschung, J., Nauels, A., Xia, Y., Bex, V., and Midgley, P. M., Cambridge University Press, Cambridge, UK and New York, NY, USA, 1535 pp., 2013.

Jones, P. W.: First- and Second-Order Conservative Remapping Schemes for Grids in Spherical Coordinates, Mon. Weather Rev., 127, 2204-2210, 10.1175/1520-0493(1999)127<2204:Fasocr>2.0.Co;2, 1999.

Jones, J. M., Fogt, R. L., Widmann, M., Marshall, G. J., Jones, P. D., and Visbeck, M.: Historical SAM Variability. Part I: Century-Length Seasonal Reconstructions, J. Climate, 22, 5319-5345, 10.1175/2009jcli2785.1, 2009

Kim, H. J.: Global Soil Wetness Project Phase 3 Atmospheric Boundary Conditions (Experiment 1), Data Integration and Analysis System (DIAS) [data set], https://doi.org/10.20783/DIAS.501/ (last access: 27 June 2022), 2017a.

Kim, J., Oh, H.-S., Lim, Y., and Kang, H.-S.: Seasonal precipitation prediction via data-adaptive principal component regression, Int. J. Climatol., 37, 75-86, https://doi.org/10.1002/joc.4979, 2017b.

Korell, L., Auge, H., Chase, J. M., Harpole, W. S., and Knight, T. M.: Responses of plant diversity to precipitation change are strongest at local spatial scales and in drylands, Nat. Commun., 12, 2489, 10.1038/s41467-021-22766-0, 2021.

Liang-Liang, L., Jian, L., and Ru-Cong, Y.: Evaluation of CMIP6 HighResMIP models in simulating precipitation over Central Asia, Adv. Clim. Change Res., 13, 1-13, https://doi.org/10.1016/j.accre.2021.09.009, 2022.

Medvigy, D. and Beaulieu, C.: Trends in Daily Solar Radiation and Precipitation Coefficients of Variation since 1984, J. Climate, 25, 1330-1339, 10.1175/2011jcli4115.1, 2012.

Meinshausen, M., Raper, S. C. B., and Wigley, T. M. L.: Emulating coupled atmosphere-ocean and carbon cycle models with a simpler model, MAGICC6 – Part 1: Model description and calibration, Atmos. Chem. Phys., 11, 1417-1456, 10.5194/acp-11-1417-2011, 2011.

Michel, S., Swingedouw, D., Chavent, M., Ortega, P., Mignot, J., and Khodri, M.: Reconstructing climatic modes of variability from proxy records using ClimIndRec version 1.0, Geosci. Model Dev., 13, 841-858, 10.5194/gmd-13-841-2020, 2020.

Nicholls, Z. R. J., Meinshausen, M., Lewis, J., Gieseke, R., Dommenget, D., Dorheim, K., Fan, C. S., Fuglestvedt, J. S., Gasser, T., Golüke, U., Goodwin, P., Hartin, C., Hope, A. P., Kriegler, E., Leach, N. J., Marchegiani, D., McBride, L. A., Quilcaille, Y., Rogelj, J., Salawitch, R. J., Samset, B. H., Sandstad, M., Shiklomanov, A. N., Skeie, R. B., Smith, C. J., Smith, S., Tanaka, K., Tsutsui, J., and Xie, Z.: Reduced Complexity Model Intercomparison Project Phase 1: introduction and evaluation of global-mean temperature response, Geosci. Model Dev., 13, 5175-5190, 10.5194/gmd-13-5175-2020, 2020.

O'Neill, B. C., Tebaldi, C., van Vuuren, D. P., Eyring, V., Friedlingstein, P., Hurtt, G., Knutti, R., Kriegler, E., Lamarque, J. F., Lowe, J., Meehl, G. A., Moss, R., Riahi, K., and Sanderson, B. M.: The Scenario Model Intercomparison Project (ScenarioMIP) for CMIP6, Geosci. Model Dev., 9, 3461-3482, 10.5194/gmd-9-3461-2016, 2016.

Prein, A. F., Rasmussen, R. M., Ikeda, K., Liu, C., Clark, M. P., and Holland, G. J.: The future intensification of hourly precipitation extremes, Nat. Clim. Change, 7, 48-52, 10.1038/nclimate3168, 2017.

https://doi.org/10.5194/gmd-2022-144
Preprint. Discussion started: 7 July 2022

Riahi, K., van Vuuren, D. P., Kriegler, E., Edmonds, J., O'Neill, B. C., Fujimori, S., Bauer, N., Calvin, K., Dellink, R., Fricko, O., Lutz, W., Popp, A., Cuaresma, J. C., Kc, S., Leimbach, M., Jiang, L., Kram, T., Rao, S., Emmerling, J., Ebi, K., Hasegawa, T., Havlik, P., Humpenöder, F., Da Silva, L. A., Smith, S., Stehfest, E., Bosetti, V., Eom, J., Gernaat, D., Masui, T., Rogelj, J., Strefler, J., Drouet, L., Krey, V., Luderer, G., Harmsen, M., Takahashi, K., Baumstark, L., Doelman, J. C., Kainuma, M., Klimont, Z., Marangoni, G., Lotze-Campen, H., Obersteiner, M., Tabeau, A., and Tavoni, M.: The Shared Socioeconomic Pathways and their energy, land use, and greenhouse gas emissions implications: An overview, Glob. Environ. Change, 42, 153-168, https://doi.org/10.1016/j.gloenvcha.2016.05.009, 2017.

Samset, B. H., Myhre, G., Forster, P. M., Hodnebrog, Ø., Andrews, T., Faluvegi, G., Fläschner, D., Kasoar, M., Kharin, V., Kirkevåg, A., Lamarque, J.-F., Olivié, D., Richardson, T., Shindell, D., Shine, K. P., Takemura, T., and Voulgarakis, A.: Fast and slow precipitation responses to individual climate forcers: A PDRMIP multimodel study, Geophys Res. Lett., 43, 2782-2791, https://doi.org/10.1002/2016GL068064, 2016.

Shepherd, T. G.: Atmospheric circulation as a source of uncertainty in climate change projections, Nat. Geosci., 7, 703-708, 10.1038/ngeo2253, 2014.

Song, F., Leung, L. R., Lu, J., and Dong, L.: Seasonally dependent responses of subtropical highs and tropical rainfall to anthropogenic warming, Nat. Clim. Change, 8, 787-792, 10.1038/s41558-018-0244-4, 2018.

Sun, Q., Miao, C., Duan, Q., Ashouri, H., Sorooshian, S., and Hsu, K.-L.: A Review of Global Precipitation Data Sets: Data Sources, Estimation, and Intercomparisons, Rev. Geophys., 56, 79-107, https://doi.org/10.1002/2017RG000574, 2018.

Trenberth, K. E., Dai, A., Rasmussen, R. M., and Parsons, D. B.: The Changing Character of Precipitation, B. Am. Meteorol. Soc., 84, 1205-1218, 10.1175/bams-84-9-1205, 2003.

Trenberth, K. E. and Shea, D. J.: Relationships between precipitation and surface temperature, Geophys. Res. Lett., 32, https://doi.org/10.1029/2005GL022760, 2005.

van Oldenborgh, G. J. and Burgers, G.: Searching for decadal variations in ENSO precipitation teleconnections, Geophys. Res. Lett., 32, https://doi.org/10.1029/2005GL023110, 2005.

Yang, X., Yong, B., Yu, Z., and Zhang, Y.: An evaluation of CMIP5 precipitation simulations using ground observations over ten river basins in China, Hydrol. Res., 52, 676-698, 10.2166/nh.2021.151, 2021.

Zelazowski, P., Huntingford, C., Mercado, L. M., and Schaller, N.: Climate pattern-scaling set for an ensemble of 22 GCMs – adding uncertainty to the IMOGEN version 2.0 impact system, Geosci. Model Dev., 11, 541-560, 10.5194/gmd-11-541-2018, 2018.

Zhang, W., Furtado, K., Wu, P., Zhou, T., Chadwick, R., Marzin, C., Rostron, J., and Sexton, D.: Increasing precipitation variability on daily-to-multiyear time scales in a warmer world, Sci. Adv., 7, eabf8021, doi:10.1126/sciadv.abf8021, 2021.

Zhou, P., Liu, Z., and Cheng, L.: An alternative approach for quantitatively estimating climate variability over China under the effects of ENSO events, Atmos. Res., 238, 104897, https://doi.org/10.1016/j.atmosres.2020.104897, 2020.

https://doi.org/10.5194/gmd-2022-144
Preprint. Discussion started: 7 July 2022

Geoscientific Model Development Discussions

Model	Modeling Center
UKESM1-0-LL	Met Office Hadley Centre and National Environmental Research Council, UK
MPI-ESM1-2-LR	Max Planck Institute for Meteorology, Germany
MIROC6	Japan Agency for Marine-Earth Science and Technology, Japan
IPSL-CM6A-LR	Institute Pierre Simon Laplace, France
GFDL-ESM4	Geophysical Fluid Dynamics Laboratory, USA
EC-Earth3	EC-Earth consortium, Europe
CanESM5	Canadian Centre for Climate Modeling and Analysis Environment and Climate Change, Canada.
CESM2	National Center for Atmospheric Research, Climate and Global Dynamics Laboratory, USA
ACCESS-ESM1-5	Commonwealth Scientific and Industrial Research Organisation, Australia

Table 1: List of the 9 employed CMIP6 models and the modeling groups providing them.

https://doi.org/10.5194/gmd-2022-144
Preprint. Discussion started: 7 July 2022

Geoscientific Model Development Discussions

Indice Label or Variable Symbol	Variable	Notes
e	ESM index	Indexes nine ESMs used (see Table 1)
i	PCA index	$i = 1$ is dominant spatial PCA, $1 \leq i \leq N_{PCA} = 10$ used
k	Spatial index	$1 \leq k \leq N_{grid}$, where $N_{grid} = 10,368$ grids
m	Month index	All calculations for each month, $1 \leq m \leq 12$
y	Year index	Index of years in periods of calibration or prediction
$T_{e,m}^{Timeseries}(k,y)$	Timeseries part of PCAs, for each location, and for temperature	Average gridded Tair of three months (month of interest plus the previous two months). Note, different timeseries calculated for each location indexed by *k*.
$U_{e,m}^{Spatial}(k,i)$	Spatial part of PCAs for temperature	A matrix of eigenvectors of the covariance matrix.
$T_{e,m}^{PCA}(y,i)$	Temporal principal components in PCAs	Timeseries representing the characteristics of global gridded Tair
$P_{e,m}^{global}(y)$	Monthly global land average precipitation for calibration	
$P_{e,m}^{grid}(k,y)$	Monthly gridded (i.e. local) precipitation for calibration	

Table 2: List of indices labels and variable symbols in the calibration.

https://doi.org/10.5194/gmd-2022-144
Preprint. Discussion started: 7 July 2022

Geoscientific Model Development Discussions

	SSP1-2.6		SSP2-4.5		SSP3-7.0		SSP5-8.5	
	ESM	PREMU	ESM	PREMU	ESM	PREMU	ESM	PREMU
ESMs average	0.29	0.16	0.58	0.45	0.69	0.76	0.96	0.96
UKESM1-0-LL	0.57	0.30	0.67	0.53	0.88	0.87	1.16	1.16
MPI-ESM1-2-LR	0.19	0.06	0.23	0.26	0.63	0.69	0.85	0.85
MIROC6	0.08	0.09	0.54	0.41	0.62	0.74	1.09	1.09
IPSL-CM6A-LR	0.48	0.27	0.73	0.56	1.05	0.90	1.25	1.25
GFDL-ESM4	0.15	-0.06	0.41	0.06	-0.13	0.03	0.04	0.03
EC-Earth3	0.13	0.18	0.63	0.72	1.14	1.21	1.67	1.69
CanESM5	0.51	0.40	1.15	0.90	1.33	1.32	1.48	1.48
CESM2	0.33	0.12	0.69	0.47	0.41	0.81	0.82	0.80
ACCESS-ESM1-5	0.18	0.08	0.21	0.18	0.28	0.25	0.28	0.27

Table 3: Trend of GLAP from ESMs average and each ESM and its corresponding emulation by PREMU during the period 2015-2100 under four scenarios. The ESMs Average represents the multi-model mean precipitation predicted by gridded temperature from 9 ESMs. Note that the unit is mm year^{-2}.

https://doi.org/10.5194/gmd-2022-144
Preprint. Discussion started: 7 July 2022

Geoscientific Model Development Discussions

Appendix 1

Acronym	Meaning
CMIP6	The 6th phase of the Coupled Model Intercomparison Project
EBM	Energy Balance Model
ESM	Earth System Model
GLAP	Global land average precipitation
GSWP3	Global Soil Wetness Project Phase 3
IMOGEN	Integrated Model Of Global Effects of climatic aNomalies （Zelazowski et al., 2018)
LCM	Lower complexity models
MAP	Mean annual precipitation
MESMER	Modular Earth System Model Emulator with spatially Resolved output (Beusch et al., 2021)
OSCAR	A compact Earth system model (See Gasser et al., 2017)
PCA	Principal Component Analysis
PREMU	A computationally efficient precipitation emulator (This study).
SSP	Shared Socioeconomic Pathway
Tair	Surface air temperature

Table A1: Table of acronyms.

505

https://doi.org/10.5194/gmd-2022-144
Preprint. Discussion started: 7 July 2022

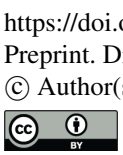

Geoscientific Model Development Discussions

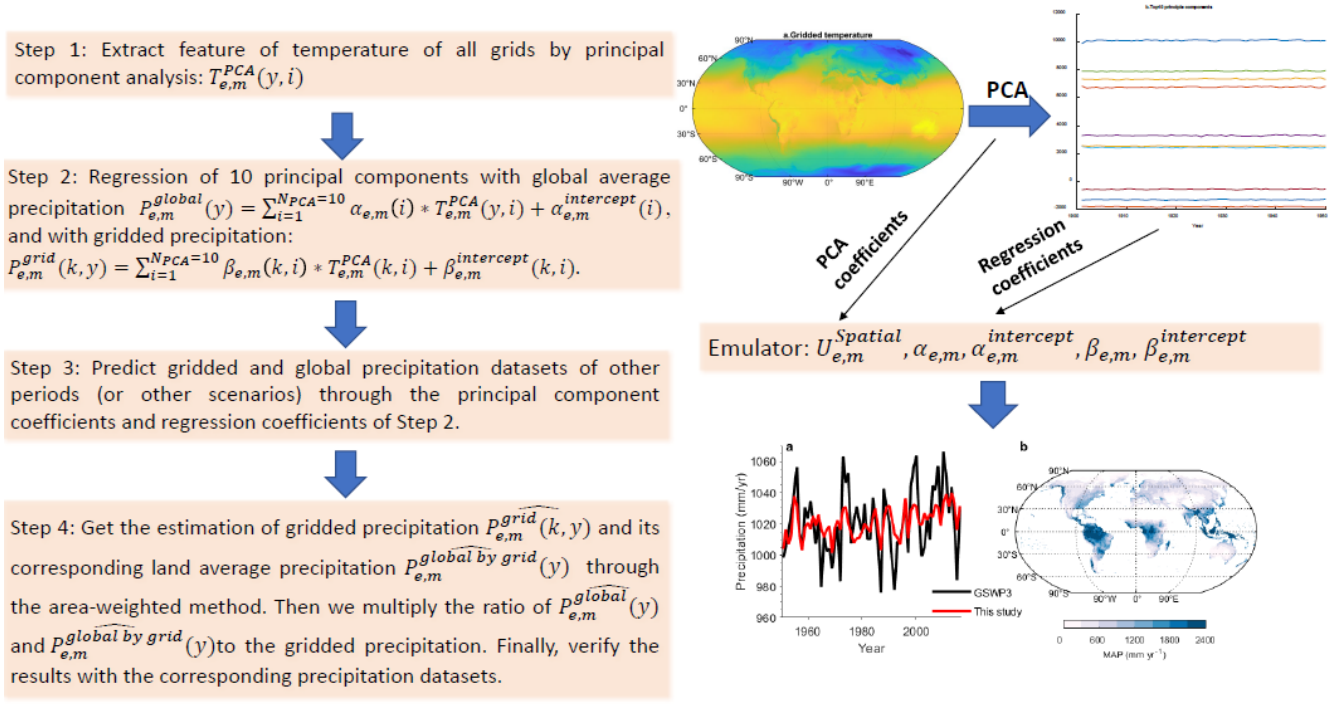

Figure 1: Illustration of the precipitation emulator driven by the gridded temperature. Step 1 is to extract the features of gridded temperature through principal component analysis. In step 2, we construct the parameters of the emulator by regression of GLAP/gridded precipitation and principal components of gridded temperature. Then we use the emulator to predict the precipitation for validation period/ scenario in Step 3. Finally, we calibrate the precipitation and verify the results with precipitation from GSWP3 and ESMs. Here, $T_{e,m}^{PCA}(y,i)$ is the principal components extracted by PCA. $P_{e,m}^{global}(y)$ is the GLAP and $P_{e,m}^{grid}(k,y)$ is the precipitation a given grid k. $\alpha_{e,m}(i)/\beta_{e,m}(k,i)$ represents the coefficients of each principal components of temperature to global/gridded precipitation and $\alpha_{e,m}^{intercept}(i)$ /$\beta_{e,m}^{intercept}(k,i)$ is the intercept term. And $U_{e,m}^{Spatial}(k,i)$ is the PCA coefficients. Note that, the gridded temperature from GSWP3 is area-weighted averaged to 2.5° x 2.5° before PCA.

https://doi.org/10.5194/gmd-2022-144
Preprint. Discussion started: 7 July 2022

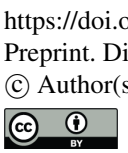

Geoscientific Model Development
Discussions
Open Access
EGU

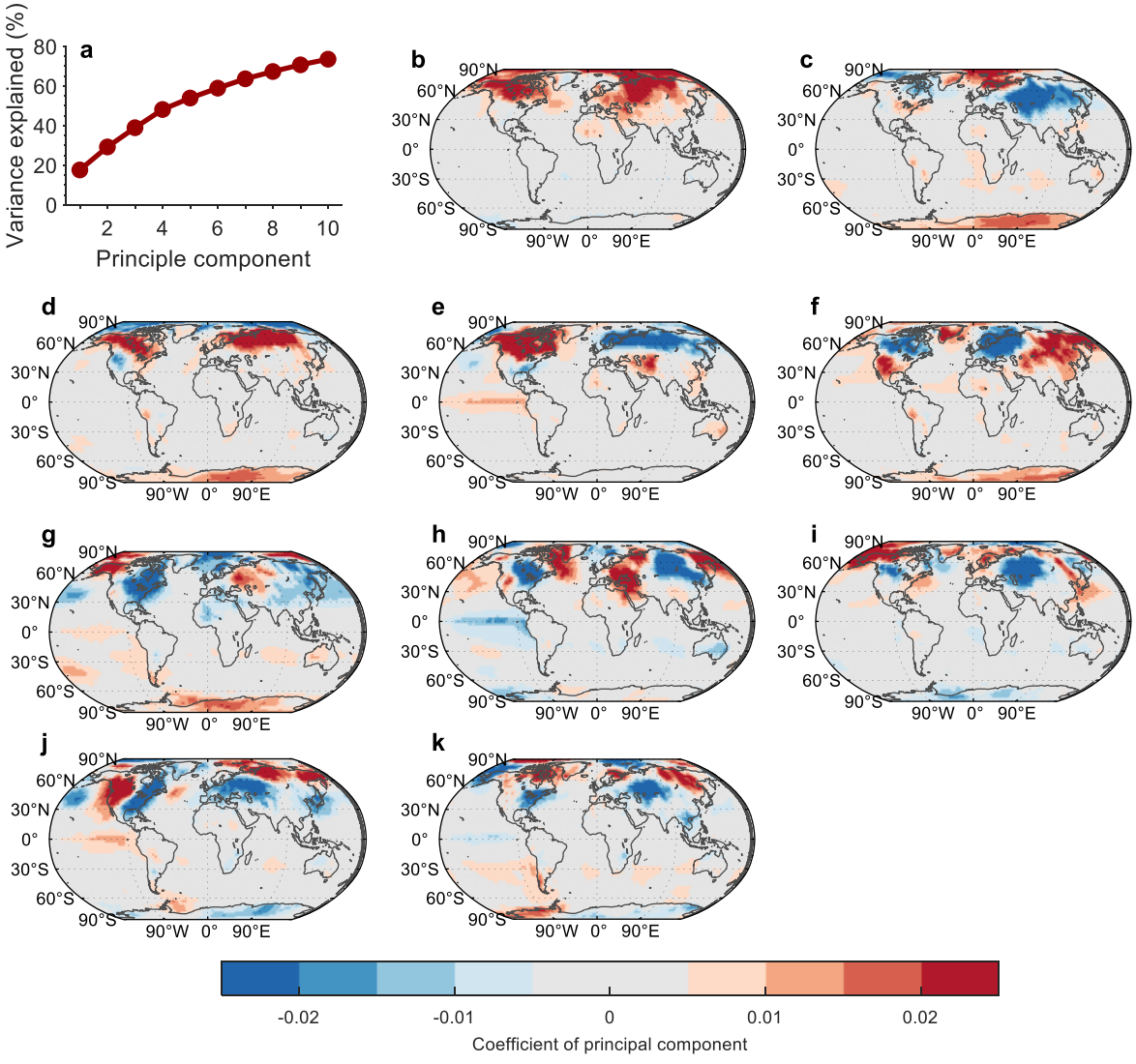

Figure 2: The corresponding results from the PCA of the gridded temperature in January between 1901 and 1950 from GSWP3: a) The cumulative variance explanation rate of the top ten principal components. b-k) Coefficients of the top ten principal components (corresponding to $U_{e,m}^{Spatial}(:,i), i = 1-10$).

https://doi.org/10.5194/gmd-2022-144
Preprint. Discussion started: 7 July 2022

Geoscientific Model Development Discussions

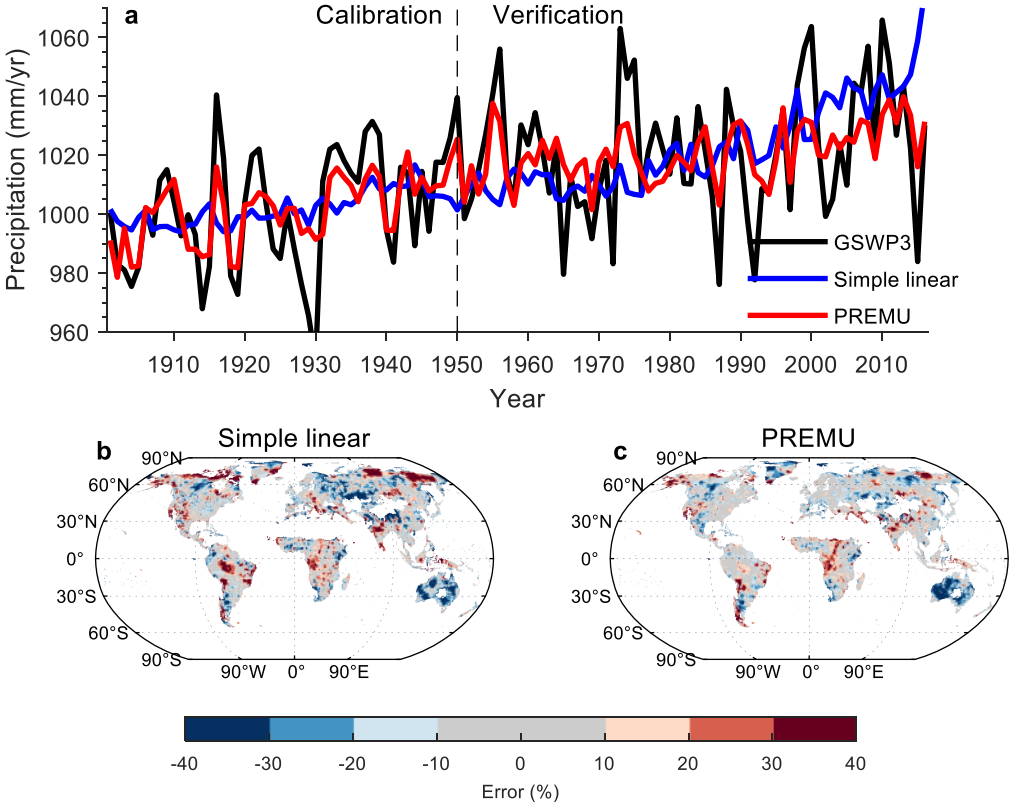

525 **Figure 3: The emulation on historical precipitation: a) GLAP of the historical observation precipitation (GSWP3), the prediction precipitation estimated by the simple linear method (Simple linear) and our emulator (PREMU) in 1901–2016. b) The spatial pattern of error of MAP in 1987-2016 between Simple linear and GSWP3. c) The spatial pattern of error of the MAP in 1987-2016 between our emulator and GSWP3. The global land average does not include Antarctica because of no emulation for Antarctica and the arid areas where the MAP from GSWP3 is less than 200 mm year^{-1} in 1980-2016 are masked.**

530

https://doi.org/10.5194/gmd-2022-144
Preprint. Discussion started: 7 July 2022

Geoscientific Model Development Discussions

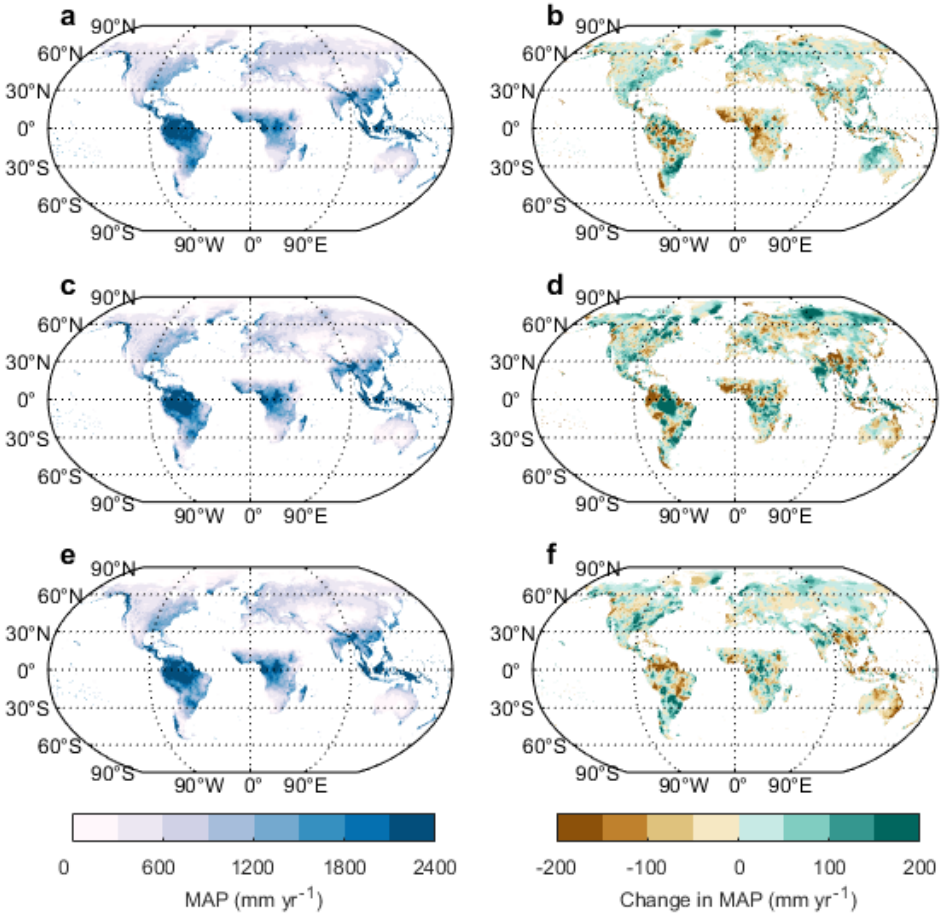

Figure 4: Spatial pattern of MAP and change in MAP: a) The MAP in 1987-2016 from GSWP3. b) The spatial pattern of change in MAP between the period of 1951-1980 and 1987-2016 from GSWP3. c-d). Same as a-b) but for the emulation from Simple linear. e-f). Same as a-b) but for the emulation from PREMU.

535

https://doi.org/10.5194/gmd-2022-144
Preprint. Discussion started: 7 July 2022

Geoscientific Model Development
Discussions
Open Access
EGU

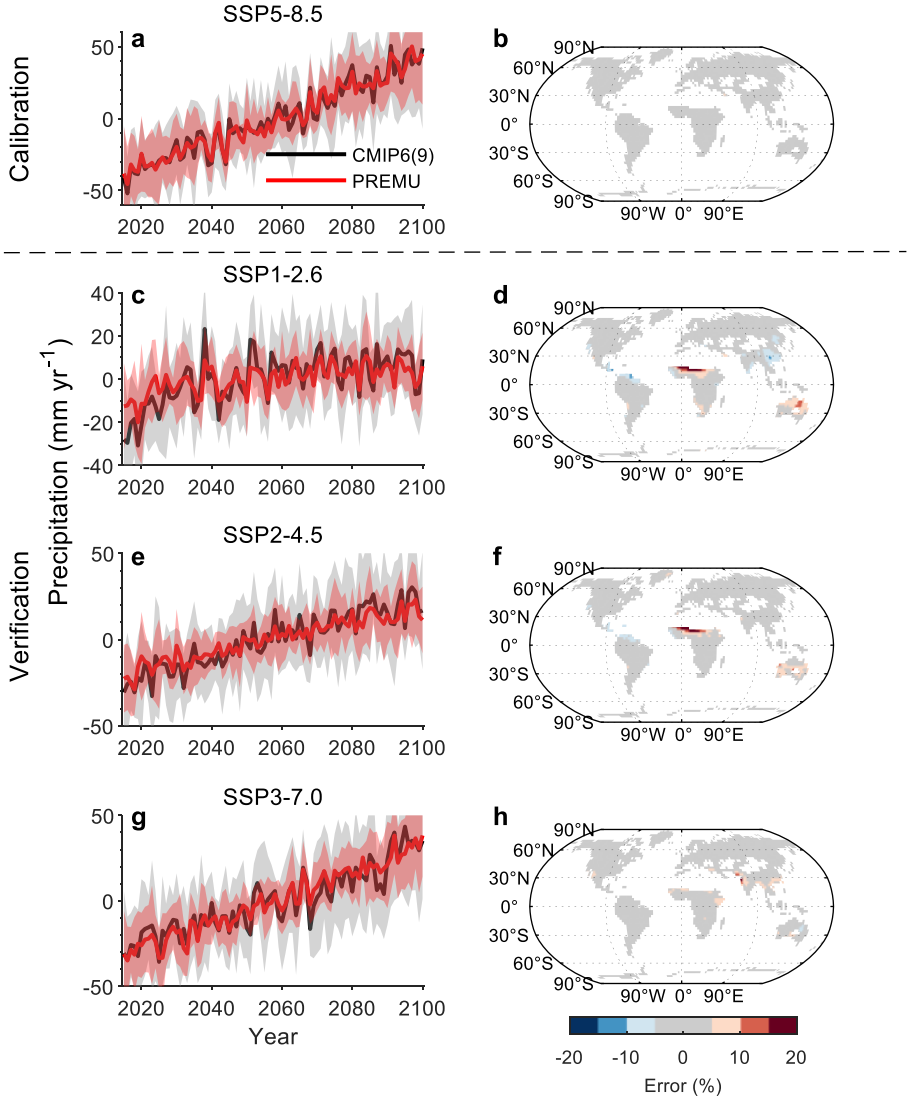

Figure 5: The emulation on future precipitation: a) multi-model mean GLAP in 9 ESMs from CMIP6 (CMIP (9)), and the precipitation prediction by our emulator (PREMU) in 2015-2100 under the SSP5-8.5 scenario. The shaded area represents the mean±std. b) The spatial pattern of error in MAP during 2071-2100 between multi-model mean and our emulator. c-d) SSP1-2.6; e-f) SSP2-4.5; g-h) SSP3-7.0.

https://doi.org/10.5194/gmd-2022-144
Preprint. Discussion started: 7 July 2022

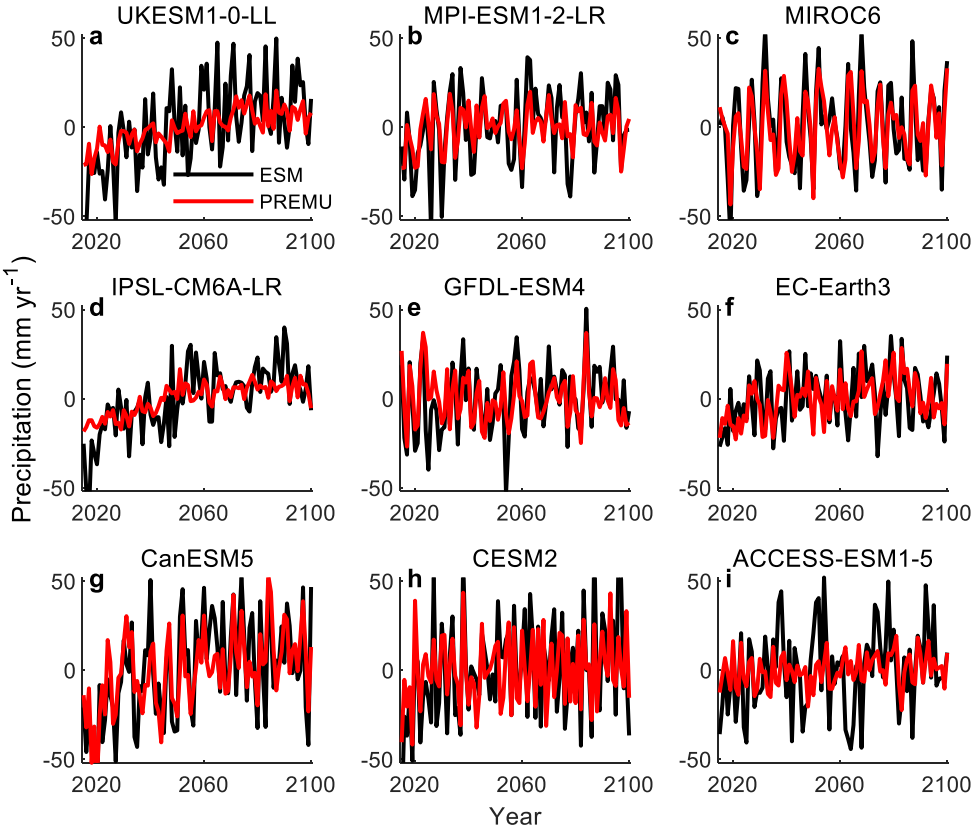

Figure 6: The anomaly of GLAP from each ESM under the SSP1-2.6 scenario: a) UKESM1-0-LL; b) MPI-ESM1-2-LR; c) MIROC6; d) IPSL-CM6A-LR; e) GFDL-ESM4; f) EC-Earth3; g) CanESM5; h) CESM2; i) ACCESS-ESM1-5.

545

https://doi.org/10.5194/gmd-2022-144
Preprint. Discussion started: 7 July 2022

Geoscientific Model Development Discussions

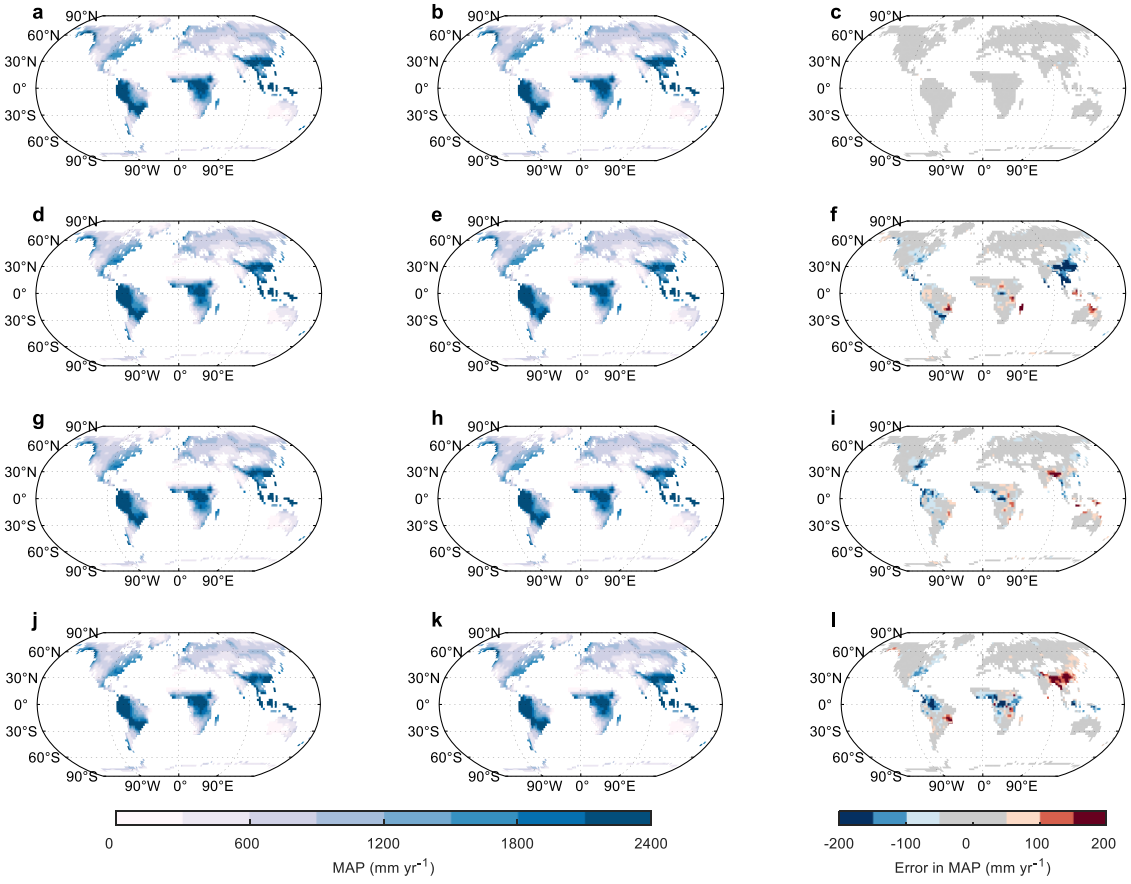

550 **Figure 7: The spatial pattern of MAP in 2071-2100 from a) multi-model mean of ESMs, b) our emulation under SSP5-8.5 scenario and c) the errors in MAP from our emulation. d-f) SSP1-2.6; g-i) SSP2-4.5; j-l) SSP3-7.0.**

https://doi.org/10.5194/gmd-2022-144
Preprint. Discussion started: 7 July 2022

Geoscientific Model Development
Discussions
Open Access
EGU

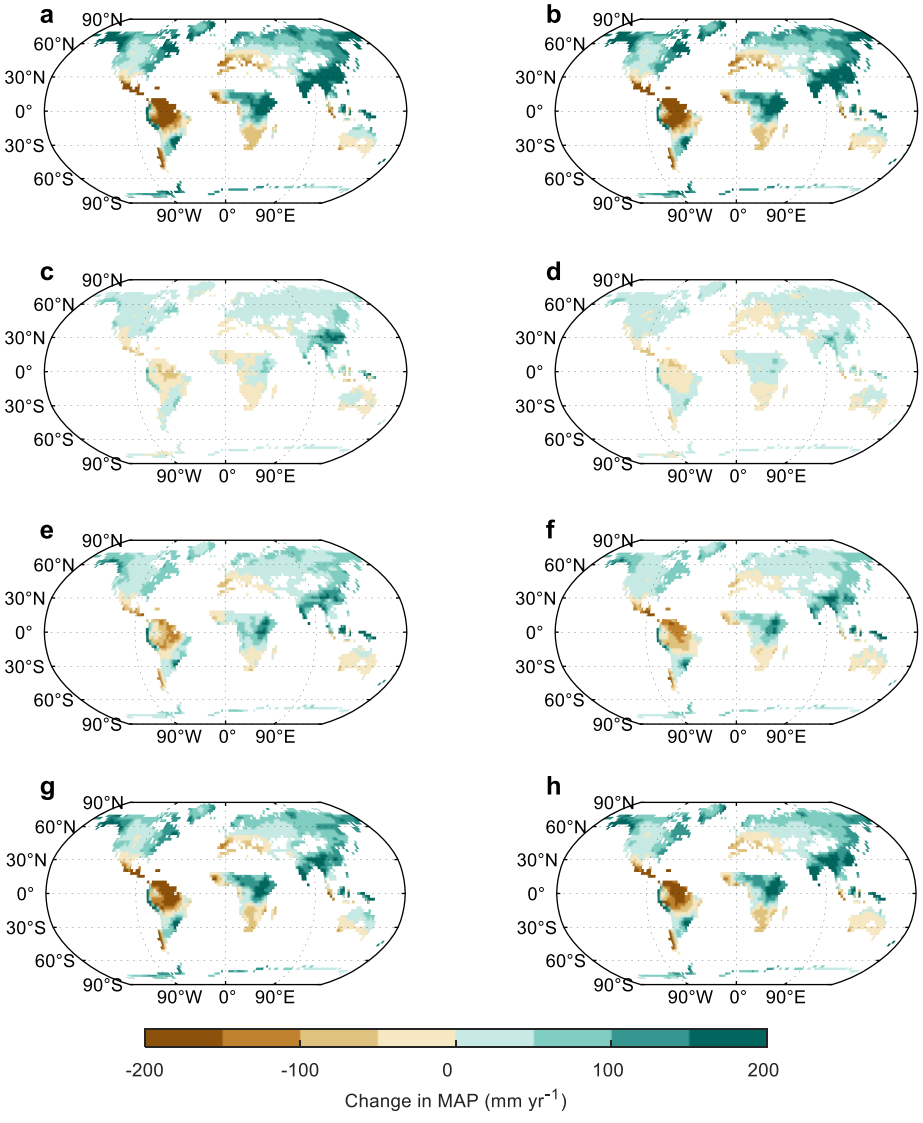

555 **Figure 8: The spatial pattern of change in MAP in 2071-2100 from a) multi-model mean of ESMs and b) our emulation under SSP5-8.5 scenario. c-d) SSP1-2.6; e-f) SSP2-4.5; g-h) SSP3-7.0.**

https://doi.org/10.5194/gmd-2022-144
Preprint. Discussion started: 7 July 2022

Geoscientific Model Development
Discussions
Open Access
EGU

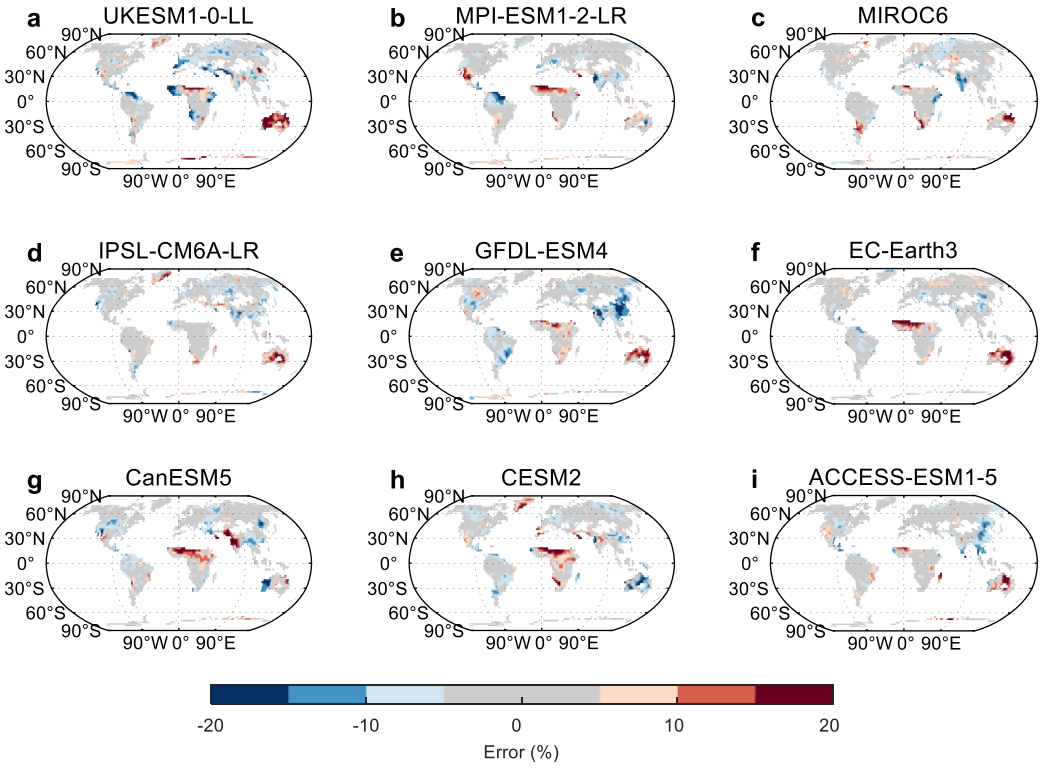

Figure 9: The spatial pattern of error of the MAP in 2071-2100 between each ESM and our emulation under the SSP1-2.6 scenario: a) UKESM1-0-LL; b) MPI-ESM1-2-LR; c) MIROC6; d) IPSL-CM6A-LR; e) GFDL-ESM4; f) EC-Earth3; g) CanESM5; h) CESM2; i) ACCESS-ESM1-5.

https://doi.org/10.5194/gmd-2022-144
Preprint. Discussion started: 7 July 2022

Geoscientific Model Development Discussions
Open Access
EGU

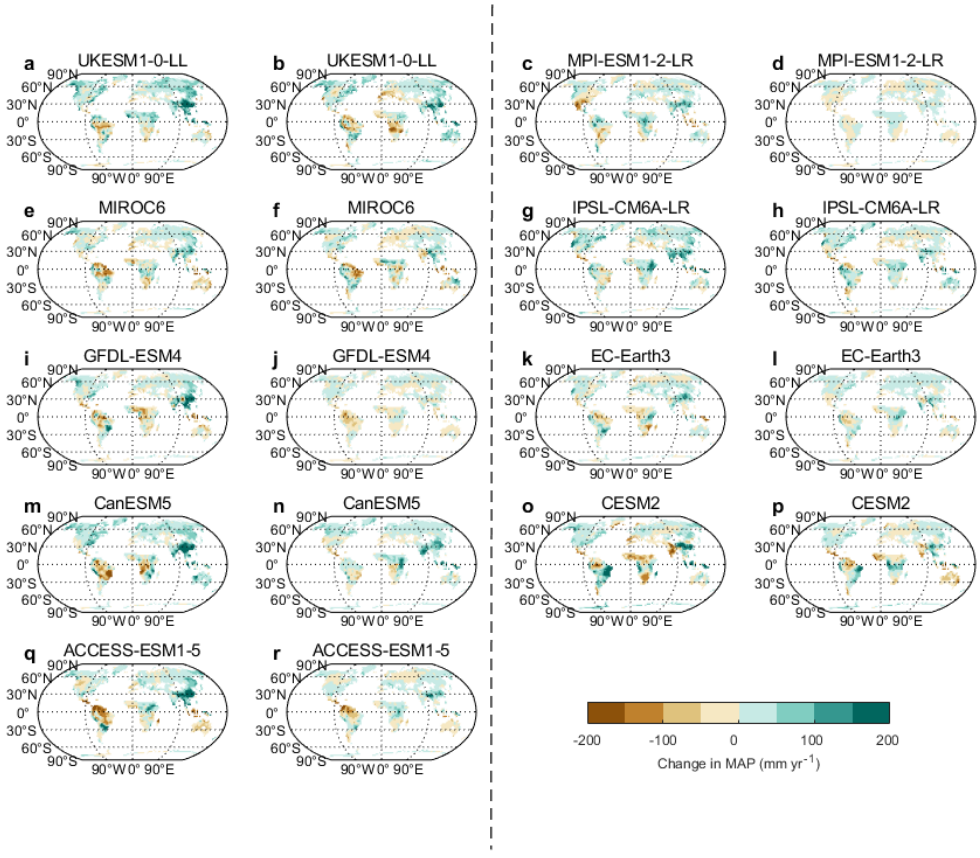

Figure 10: The spatial pattern of change in MAP between the period of 2016-2045 and 2071-2100 from a) UKESM1-0-LL and b) our emulation under SSP1-2.6 scenario. c-d) MPI-ESM1-2-LR; e-f) MIROC6; g-h) IPSL-CM6A-LR; i-j) GFDL-ESM4; k-l) EC-Earth3; m-n) CanESM5; o-p) CESM2; q-r) ACCESS-ESM1-5.